

Agriculture, Ecosystems and Environment

DSDMA: Dynamic Spray Drift Mitigation Algorithm for Optimal UAV Spraying in Agriculture

--Manuscript Draft--

Manuscript Number:	AGEE47942
Article Type:	Research Paper
Keywords:	Precision agriculture; Wind drift; Unmanned Aerial Vehicles; Spray optimization
Corresponding Author:	Rajni Goyal, Ph.D* Sant Longowal Institute of Engineering and Technology sangrur, Punjab INDIA
First Author:	Rajni Goyal, Ph.D*
Order of Authors:	Rajni Goyal, Ph.D* Srinjoy Chakraborty Amar Nath, PhD Utkarsh Niranjan, PhD
Manuscript Region of Origin:	INDIA
Abstract:	Spray drift caused by wind remains a major challenge in UAV-based agricultural spraying, often resulting in off-target contamination, reduced application efficiency, and environmental pollution. To address this issue, this study proposes an aerodynamic-based framework to ensure precise and effective agrochemical deposition. Central to this framework is the Dynamic Spray Drift Mitigation Algorithm (DSDMA), which dynamically adjusts UAV waypoints in real time by incorporating wind parameters—such as speed, direction, and flow regimes (laminar, transitional and turbulent)—to proactively correct droplet displacement before it occurs. To stabilize the UAV's trajectory under varying wind conditions, a Proportional-Integral-Derivative (PID) controller is integrated into the system. This controller effectively compensates for positional errors caused by wind-induced drag forces, ensuring improved path tracking during spraying operations. The complete framework is validated in a high-fidelity simulation environment built on AirSim, ROS2, PX4, and Unreal Engine, offering realistic aerodynamic and flight dynamics. Simulation results demonstrate that DSDMA significantly reduces spray drift, as measured by the Mean Absolute Error (MAE) between the intended and actual droplet impact points. Specifically, the MAE was 5.56 at a wind speed of 1.5 m/s, increasing to 24.56 at 7.0 m/s, indicating the growing influence of drift at higher wind velocities. Nonetheless, the algorithm exhibits strong adaptability across different wind intensities, highlighting its robustness and accuracy. The proposed framework advances UAV spraying by enabling real-time, wind-aware corrections, thus promoting environmental sustainability, regulatory compliance, and precision agriculture. This work lays the foundation for next-generation intelligent spraying systems, with potential for future expansion through AI integration, large-scale field deployments, and performance evaluations under more complex environmental conditions.

April 15, 2025

Editorial Department

Agriculture, Ecosystems and Environment

Dear Editor,

I am pleased to submit our manuscript titled “**DSDMA: Dynamic Spray Drift Mitigation Algorithm for Optimal UAV Spraying in Agriculture**” for your consideration in *Agriculture, Ecosystems and Environment*. This study presents a novel aerodynamic-based approach to address a persistent challenge in precision agriculture—**spray drift caused by wind during UAV-based chemical spraying**.

Key contributions of our study include:

1. **Dynamic Spray Drift Mitigation Algorithm (DSDMA):** We introduce an algorithm that adjusts UAV waypoints in real time using wind speed, direction, and flow regime data to proactively correct droplet drift before it occurs.
2. **Integration of Aerodynamics and Control Theory:** DSDMA is complemented by a PID controller that enhances flight stability and path accuracy under variable wind conditions, ensuring precise agrochemical deposition.
3. **High-Fidelity Simulation Validation:** The algorithm is evaluated in a comprehensive simulation environment built on AirSim, ROS2, PX4, and Unreal Engine. Results demonstrate significant reductions in spray drift, quantified via Mean Absolute Error (MAE), validating its effectiveness in laminar wind flow scenarios.
4. **Toward Sustainable and Intelligent Agriculture:** Our work promotes environmental sustainability, reduces chemical overuse, and supports regulatory compliance by improving spray targeting accuracy. It also lays the foundation for future integration with AI-based decision systems and deployment under more complex field conditions.

We believe this manuscript aligns well with the journal’s scope, particularly in the domains of UAV applications, precision agriculture, and autonomous systems. The work offers both scientific novelty and practical impact for advancing smart farming technologies.

We confirm that the manuscript is original, not previously published, and not under consideration elsewhere. We sincerely hope you find it suitable for publication, and we welcome the opportunity to address any comments or suggestions from reviewers.

Thank you for your time and consideration.

Yours Sincerely,

Rajni Goyal

Corresponding Author

Sant Longowal Institute of Engineering & Technology

Longowal, Distt. Sangrur, Punjab, India (148106)

Highlights:

1. A novel framework is generated to dynamically adjust UAVs' position based on real-time wind parameters, enhancing droplet accuracy and minimizing off-target contamination.
2. **Dynamic Spray Drift Mitigation Algorithm (DSDMA)** inspired by aerodynamics is proposed to mitigate wind effect.
3. A **PID controller** is integrated to ensure robust trajectory tracking under varying wind conditions, significantly reducing positional errors caused by wind-induced drag.
4. The framework is validated using a comprehensive simulation setup incorporating **AirSim, ROS2, PX4, and Unreal Engine**, offering realistic drone and aerodynamic behavior.
5. Simulation results demonstrate effective drift reduction, with MAE increasing proportionally with wind speed—from **5.56 m at 1.5 m/s** to **24.36 m at 7.0 m/s**—showing the algorithm's adaptability and reliability across varying wind intensities.

DSDMA: Dynamic Spray Drift Mitigation Algorithm for Optimal UAV Spraying in Agriculture

Rajni Goyal*, Srinjoy Chakraborty, Amar Nath, Utkarsh Niranjan

*Sant Longowal Institute of Engineering and Technology, SLIET
Longowal, Sangrur, 148106, Punjab, India*

Abstract

Spray drift caused by wind remains a major challenge in UAV-based agricultural spraying, often resulting in off-target contamination, reduced application efficiency, and environmental pollution. To address this issue, this study proposes an aerodynamic-based framework to ensure precise and effective agrochemical deposition. Central to this framework is the **Dynamic Spray Drift Mitigation Algorithm (DSDMA)**, which dynamically adjusts UAV waypoints in real time by incorporating wind parameters—such as speed, direction, and flow regimes (laminar, transitional and turbulent)—to proactively correct droplet displacement before it occurs. To stabilize the UAV's trajectory under varying wind conditions, a Proportional-Integral-Derivative (PID) controller is integrated into the system. This controller effectively compensates for positional errors caused by wind-induced drag forces, ensuring improved path tracking during spraying operations. The complete framework is validated in a high-fidelity simulation environment built on AirSim, ROS2, PX4, and Unreal Engine, offering realistic aerodynamic and flight dynamics. Simulation results demonstrate that DSDMA significantly reduces spray drift, as measured by the Mean Absolute Error (MAE) between the intended and actual droplet impact points. Specifically, the MAE was 5.56 at a wind speed of 1.5 m/s, increasing to 24.56 at 7.0 m/s, indicating the growing influence of drift at higher wind velocities.

*Corresponding author

Email addresses: rajni_pcs2103@sliet.ac.in (Rajni Goyal),
c02srinjoy@gmail.com (Srinjoy Chakraborty), amarnath@sliet.ac.in (Amar Nath),
utkarsh@sliet.ac.in (Utkarsh Niranjan)

Nonetheless, the algorithm exhibits strong adaptability across different wind intensities, highlighting its robustness and accuracy.

The proposed framework advances UAV spraying by enabling real-time, wind-aware corrections, thus promoting environmental sustainability, regulatory compliance, and precision agriculture. This work lays the foundation for next-generation intelligent spraying systems, with potential for future expansion through AI integration, large-scale field deployments, and performance evaluations under more complex environmental conditions.

Keywords: Precision agriculture, Wind drift, Unmanned Aerial Vehicles, Spray optimization, Spray drift, and Drone simulation.

1. Introduction

The growing global population and economic development fuel an unprecedented demand for increased food production. Meeting this demand will require a 70% rise in agricultural yields over the next three decades (Alexandratos et al. , 2012). Agrochemicals such as pesticides and fertilizers are widely used to enhance crop productivity. However, their excessive application poses significant risks to human health and the environment. While eliminating agrochemicals entirely is impractical, optimizing their deployment through precision agriculture can mitigate these risks. Among new technologies, spray drones or Unmanned Aerial Vehicles (UAVs) are a promising option for effective and specific agrochemical spraying.

In spite of their benefits, a major challenge of wind-borne spray drift exists. It leads agrochemicals away from their desired target, as in Fig. 1. This drift lowers spraying efficiency and pollutes non-target sites, such as water bodies, neighboring crops, and ecosystems (Sánchez et al., 2023). Reducing drift is therefore necessary to provide precision, cost-effectiveness, and environmental protection in UAV-based spraying.

Spray drift is governed by a combination of controllable (operational) and uncontrollable (environmental) parameters. Controllable factors include UAV operational parameters such as nozzle type, droplet size, release height, and flight speed, while uncontrollable factors encompass environmental conditions like wind speed, temperature, and humidity (Felsot et al. , 2010). While drift cannot be completely eliminated, it can be significantly reduced through optimal UAV configurations and adaptive spraying techniques. Previous research has addressed drift reduction by manipulating controllable

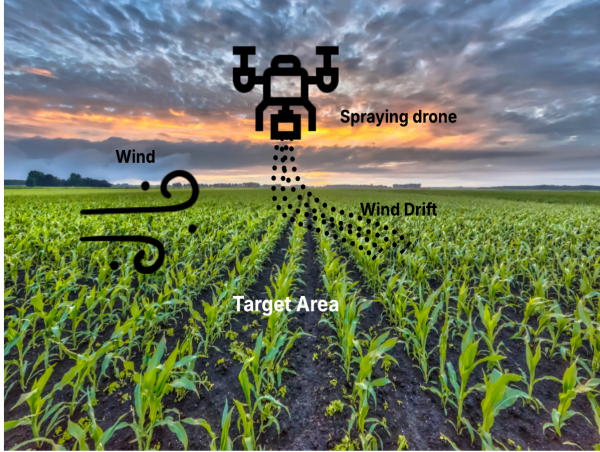


Fig. 1: Wind-induced spray drift resulting in off-target application.

parameters. As an example, (Wang et al., 2020a) tested centrifugal and hydraulic nozzles in a wind tunnel, illustrating that they have greater risks of drift with the same-sized droplets. In a parallel experiment, (Wang et al., 2020b) concluded that low droplets in high wind increase drift even at downwind distances. While these studies optimized UAV configurations (e.g., nozzle selection, flight speed), they largely ignored real-time environmental variability, limiting their field applicability.

State-of-the-art real-time spray drift mitigation solutions now incorporate dynamic UAV control algorithms that actively compensate for wind variations during operation. Faiçal et al. (Faiçal et al., 2017) developed an adaptive control system that modifies flight paths based on weather data, improving pesticide deposition. However, their approach struggles in high-wind scenarios and lacks validation in real-world farming environments. Similarly, Chen et al. (Chen et al., 2019) proposed a fuzzy logic-based system, reducing drift by 33.7% in controlled tests, but its responsiveness to sudden wind fluctuations remains inadequate.

Another study (Scagnellato, 2022) integrated aerodynamic drift models into UAV guidance systems, enhancing wind adaptability. Yet, computational inefficiencies and incomplete aerodynamic considerations hinder their scalability. Meanwhile, (An et al., 2023) explored a UAV-based methane emission suppression approach, FADE-MAS2D, for swarming drones and anomalous diffusion modeling to detect and control soil methane emissions via biochar mulch spreading. The author used aerodynamics but overlooked

49 dynamic wind-flow regimes for high wind speeds(turbulent and transitional),
50 restricting broader implementation. While much progress has been made
51 with UAV-based spraying and emission regulation, a number of fundamental
52 issues still remain. Numerous current systems do not possess sufficient
53 real-time responsiveness, being generally unable to adapt to unexpected gusts
54 and similar sudden wind alterations. Also, computational inefficiency is an
55 existing bottleneck because elaborate algorithms introduce delays that can
56 affect timely decision-making. A second limitation is the overly simplified
57 aerodynamic modeling, where transitional and turbulent wind flows are often
58 ignored, resulting in lower accuracy in real-world applications.

59 To efficiently address the aforementioned gaps and to counteract
60 wind-induced spray drift in UAV-based agrochemical applications, this
61 research suggests the **Dynamic Spray Drift Mitigation Algorithm**
62 (**DSDMA**)—a real-time adaptive control mechanism aimed at optimizing
63 UAV flight trajectories and spraying patterns according to current wind
64 conditions. In contrast to traditional static spraying techniques, DSDMA
65 adapts dynamically by categorizing wind conditions into laminar, transitional,
66 and turbulent regimes. Aerodynamic considerations are subsequently
67 employed to calculate drag forces in each regime, while kinematic relations
68 approximate the displacement of the drone from its desired trajectory. This
69 categorization enables precise wind compensation, leading to uniform droplet
70 deposition and reduced drift losses

71 Moreover, Proportional-Integral-Derivative (PID) controller (Li et al.,
72 2006) is also incorporated within the system so that UAV tracks a specified
73 target (e.g., position, velocity, or orientation) by constantly modifying its
74 control inputs following the deviation between the target state and its current
75 state. Utilizing a ROS2-AirSim-PX4 SITL simulation environment, the
76 algorithm is thoroughly validated under various environmental conditions
77 with high fidelity in simulating real-world agricultural spraying operations.

78 This study bridges the gap between theoretical aerodynamic modeling
79 and practical UAV field deployment, offering a scalable and computationally
80 efficient solution for precision agriculture. The remainder of this paper
81 presents a detailed discussion on the algorithmic design(Section 3), simulation
82 framework(Section 4), and performance evaluation(Section 5), demonstrating
83 the effectiveness of DSDMA in reducing spray drift and enhancing
84 agrochemical application accuracy.

85 **2. Material and methods**

86 *2.1. Aerodynamic Drag and Spray Dispersion*

87 Aerodynamics is the study of air interaction with the solid objects moving
88 through it. It analysis the forces like lift, drag, thrust, and gravity influencing
89 motion. When spraying in agricultural environments using UAVs, wind can
90 significantly affect the trajectory of spray droplets as well as drone. The
91 force exerted by wind causes the droplets to drift away from their intended
92 target, reducing the effectiveness of the spraying operation. To mitigate this
93 effect, it is essential to calculate the optimal spray position of the drone
94 by accounting for wind speed, direction, and the resulting drag force on
95 the droplets (Anderson, 2011). Drag force is the resistance experienced by
96 an object moving through air. This force opposes the object's motion and
97 limits its maximum terminal velocity. Drag can occur in laminar, turbulent,
98 or transitional, depending on the flow conditions. In laminar flow, the air
99 moves in smooth, parallel layers, resulting in a predictable flow pattern
100 essential for accurate droplet placement. The drag force acting on a spherical
101 droplet in that laminar flow regime can be calculated using Stokes' drag law
102 equation 1 (Greenblatt and Williams, 2022; An et al., 2023).

$$f_{wl} = 6\pi\eta r \times V \quad (1)$$

103 Where: f_{wl} is the drag force for laminar, η is the dynamic viscosity of air, r
104 is the droplet radius, and V is the wind speed.

105 However, in turbulent flow conditions, the fluid moves chaotically and
106 unpredictably, with swirling patterns and rapid changes in speed and direction.
107 The wind speed is much stronger than the fluid's natural resistance (thickness
108 or stickiness). In this case, the aerodynamic drag force acting on the moving
109 vehicle moving through the air is calculated using Equation 2, Bagchi et al.
110 (2003).

$$f_{wt} = \frac{1}{2} C_d \rho_{air} S V^2 \quad (2)$$

111 Where: f_{wt} denotes the drag force for turbulent flow, C_d denotes the drag
112 coefficient, ρ_{air} represents the air density, S signifies the cross-sectional area
113 V represents the wind velocity.

114 However, when the flow is transitional, the drag force is not purely governed
115 by Stokes' law (laminar flow) or the turbulent drag equation. Instead, it is
116 an intermediate state where laminar and turbulent flow characteristics may

117 coexist. In this case, the drag force is typically expressed using a combination
 118 of empirical formulas or approximations (Birouk and Abou Al-Sood, 2007).
 119 The drag coefficient C_d is taken as a function of the Reynolds number (Re),
 120 interpolating between the laminar and turbulent regimes (Clift et al., 2005)
 121 (Equation 3), and the drag force is calculated using equation 2.

$$C_d = 24 \left(\frac{1}{Re} + 0.15Re^{0.687} \right) \quad (3)$$

122 **Reynold's Number:**

123 To decide the nature of the fluid flow (laminar, transitional, and
 124 turbulent regimes), a dimensionless and key parameter named Reynolds
 125 number(Re) (Genç, 2012) is used. The Reynolds number is calculated using
 126 the equation 4.

$$Re = \frac{\rho \cdot V \cdot D}{\mu} \quad (4)$$

127 Where: Re is the Reynolds number, ρ is the fluid (wind) density (kg/m^3),
 128 V is the fluid velocity (wind velocity) (m/s), D is the characteristic length
 129 (diameter of the droplet or object, in meters) and μ is the dynamic viscosity
 130 of the fluid ($\text{kg}/(\text{m}\cdot\text{s})$).

131 Table 1 shows the relation between flow type and Reynolds number.

Flow Type	Reynolds Number	Wind Speed Relationship
Laminar Flow	$Re < 2000$	Low wind speed
Transitional Flow	$2000 < Re < 4000$	Moderate wind speed
Turbulent Flow	$Re > 4000$	High wind speed

Table 1: Relationship between flow type, Reynolds number, and wind speed

132 So, by calculating the drag force depending upon the regimes, the
 133 displacement of the spray from the target can be calculated using the kinematic
 134 equation (Bottema and Roth, 1990).

135 *2.1.1. Mathematical framework for aerodynamic drags*

136 The drone's initial position is defined by x and y coordinates. When wind
 137 is introduced, it alters the trajectory of the agrochemical spray, causing it to
 138 deviate from its intended path. This deviation is measured as displacements

139 x_m and y_m in the x and y directions, respectively. This framework
 140 calculates the optimal drone position to ensure the spray lands accurately on
 141 the target, compensating for the effects of aerodynamic drag.

142 To account for the effect of wind, the target positions x and y are adjusted
 143 by adding the wind-induced displacements and changing the control law as
 144 per Equation 5.

$$\rho(x, y, t) \rightarrow \rho(x_m, y_m, t) \quad (5)$$

145 Where,

$$x_m = x^* + V_x \quad (6)$$

$$y_m = y^* + V_y \quad (7)$$

146 Here, V_x and V_y represent the wind speed components in the horizontal
 147 (x) and vertical (y) directions, respectively. The wind speed and direction
 148 are typically measured in polar coordinates (speed and direction in degrees).
 149 To analyze the wind's influence on the spray's trajectory, these components
 150 are decomposed into cartesian coordinates:

$$V_x = V \cdot \cos(\theta) \quad (8)$$

$$V_y = V \cdot \sin(\theta) \quad (9)$$

152 Here, V is the wind speed, and θ is the wind direction in radians.

153 The spray droplet's displacement due to wind during its fall is computed
 154 by integrating the effects of wind speed and drag force over time and is
 155 expressed by the following kinematic equations.

$$x^* = 0.5 \times (f_{w_x} \times t^{*2}) + (V_x \times t^*) + x_0 \quad (10)$$

$$y^* = 0.5 \times (f_{w_y} \times t^{*2}) + (V_y \times t^*) + y_0 \quad (11)$$

156 These equations consider the acceleration due to drag and the constant
 157 influence of wind velocity. x_0 and y_0 represent the initial coordinates of the
 158 spray target. t^* is the time it takes for a droplet to fall from a given height h
 159 to the ground under the influence of gravity and is calculated as:

$$t^* = \sqrt{\frac{2h}{g}} \quad (12)$$

160 Here, g represents the acceleration due to gravity. This time t^* is critical
 161 to determining how long the wind will influence the trajectory of the droplet.
 162 **Laminar flow:** The drag force is decomposed into its x and y components
 163 according to equations 13 and 14 for laminar.

$$f_{wx} = 6\pi\eta r \times V_x \quad (13)$$

$$f_{wy} = 6\pi\eta r \times V_y \quad (14)$$

164 Where f_w is the drag force, η is the dynamic viscosity of air, r is the
 165 radius of the droplet, and V is the wind speed.

166 **Turbulent flow:** For turbulent flow (high Reynolds numbers), drag force is
 167 not linearly dependent on velocity. The drag force in turbulent conditions is
 168 usually modeled by Equation 2. The velocity of the droplet in the direction
 169 of the wind is updated iteratively to account for the effect of drag force. The
 170 new velocity $V_x(\text{new})$ is calculated as:

$$V_x(\text{new}) = V_x(\text{old}) - \frac{F_d}{m} \Delta t \quad (15)$$

171 where: F_d drag force, m mass of the droplet, Δt small time step for
 172 numerical integration.

173 The total displacement of the droplet (x_{drag}) due to wind is calculated
 174 incrementally using the updated velocity:

$$x_{\text{drag}}+ = V_x \Delta t \quad (16)$$

175 This process is repeated for each time step, updating the droplet's velocity
 176 based on the drag force and calculating the new displacement after each
 177 iteration. Over time, the accumulated displacement will give the total drift
 178 of the droplet away from the target area.

179 **Transitional flow:** This is the intermediate state, when the wind speed is
 180 average, neither high nor low. The spray drift due to wind is calculated using
 181 turbulent drag force. However, the drag coefficient C_d is computed using
 182 Equation 3.

183 *2.2. Proportional-Integral-Derivative (PID) controller*

184 When wind conditions (speed and direction) remain constant during
 185 spraying, pre-calculating the drone's optimal position based on aerodynamic

186 drag is sufficient to ensure precise spray delivery. However, in real-world
 187 agricultural environments, wind conditions are often unpredictable, causing
 188 fluctuations in speed and direction. Under such varying conditions,
 189 aerodynamic drag alone cannot maintain accuracy. As a result, both the
 190 spray droplets and the drone itself may deviate from their intended paths,
 191 leading to ineffective spraying and potential crop damage.

192 To address this challenge, a Proportional-Integral-Derivative (PID)
 193 controller was integrated into the droplet displacement model. The PID
 194 controller helps mitigate positional errors caused by wind-induced drag forces,
 195 ensuring that the drone can dynamically adjust its position in real time. It is
 196 calculated using equation 17.

$$u[k] = K_p e[k] + K_i \sum_{i=0}^k e[i] \Delta t + K_d \frac{e[k] - e[k-1]}{\Delta t} \quad (17)$$

197 Where: $u(t)$: Control output at time t , $e(t)$: Error, i.e., the difference
 198 between the desired setpoint and the actual process variable, K_p : Proportional
 199 gain, K_i : Integral gain, K_d : Derivative gain and Δt : Time step interval (for
 200 discrete PID).

201 Given that significant displacement primarily occurs in transitional and
 202 turbulent flow regimes, the PID control strategy was explicitly applied to these
 203 cases. For computational efficiency, only the proportional term ($K_p = 1.2$)
 204 was utilized for real-time corrections, while the integral (K_i) and derivative
 205 (K_d) terms were set to zero. This simplification reduces processing overhead
 206 while maintaining effective control, leading to the modified PID equation
 207 (Equation 18).

$$u_x^{\text{prop}}(t) = K_p e_x(t). \quad (18)$$

208 The error $e_x(t)$ is the difference between the desired position
 209 ($x_{\text{desired}}, y_{\text{desired}}, z_{\text{desired}}$) and the current position ($x_{\text{current}}, y_{\text{current}}, z_{\text{current}}$) of
 210 the drone along the three axis:

$$e_x(t) = x_{\text{desired}} - x_{\text{current}}, \quad (19)$$

$$e_y(t) = y_{\text{desired}} - y_{\text{current}}, \quad (20)$$

$$e_z(t) = z_{\text{desired}} - z_{\text{current}}. \quad (21)$$

211 The proportional term ($K_p e(t)$) applies an immediate correction
 212 proportional to the current error. If wind pushes the UAV off course, the
 213 proportional term moves the UAV back toward the desired trajectory. The
 214 total control signal for each axis is the sum of all three terms:

$$u_x(t) = u_x^{\text{prop}}(t) \quad (22)$$

$$u_y(t) = u_y^{\text{prop}}(t) \quad (23)$$

$$u_z(t) = u_z^{\text{prop}}(t). \quad (24)$$

215 The control outputs ($u_x(t), u_y(t), u_z(t)$) are used to adjust the UAV's
 216 position dynamically:

$$x_{\text{new}} = x_{\text{current}} + u_x(t)\Delta t, \quad (25)$$

$$y_{\text{new}} = y_{\text{current}} + u_y(t)\Delta t, \quad (26)$$

$$z_{\text{new}} = z_{\text{current}} + u_z(t)\Delta t, \quad (27)$$

217 Where Δt is the update time step. These adjustments ensure the UAV
 218 maintains its desired trajectory, compensating for wind-induced drift.

219 Integrating the PID controller significantly improved the UAV's ability to
 220 maintain its intended trajectory under varying wind conditions. The simplicity
 221 of the proportional control mechanism ensured computational efficiency while
 222 preserving accuracy, making it suitable for real-time agricultural operations.

223 3. Proposed DSDMA Algorithm

224 The proposed DSDMA (Algorithm 1) is designed to optimize the spraying
 225 operation of a drone in agricultural environments by dynamically adjusting
 226 its position and spraying mode based on real-time wind conditions. Initially,
 227 the drone operates using a pre-loaded map of the target weed locations (here
 228 assumed to be a square field with four weed locations at each corner).

229 The goal is to mitigate the impact of wind on the spray of agrochemicals,
 230 ensuring that the target locations of the weeds receive the intended treatment
 231 while minimizing the drift caused by the wind. The algorithm takes wind
 232 speed V and wind direction θ as input parameters, and other parameters
 233 such as nozzle radius, air's dynamic viscosity, drag coefficient, gravity, and air
 234 density are pre-defined parameters and used for drift calculations. Initially,
 235 the drone is set to Flying state, leaving the base station to begin its spraying
 236 operation. The spray mode is set to be Normal Spray Mode for spraying.

Algorithm 1: DSDMA: Dynamic Spray Drift Mitigation Algorithm

1 **Input:** Wind speed (V) and direction (θ).
 2 **Constants:** Droplet radius: $r = 0.0002$ m, Dynamic viscosity of air: $\eta = 1.81 \times 10^{-5}$ Pa·s, Drag coefficient (Laminar): $C_d = 0.0679$, Air density: $\rho_{\text{air}} = 1.225$ kg/m³, Spray liquid density: $\rho_{\text{fertilizer}} = 1000$ kg/m³, Acceleration due to gravity: $g = 9.81$ m/s², Drone speed: $V_{\text{drone}} = 5$ m/s, Flight height: $h = 20$ m, Flight time: $t_{\text{flight}} = h/V_{\text{drone}}$
 3 **Initialization:** The drone departs from its base station to commence the spraying operation.
 4 **Drone State:** FLYING
 5 **Spray Mode:** NORMAL
 6 The drone navigates to the mapped weed locations and transitions its state:
 7 **Drone State:** EXPLORATION
 8 **if** *Drone reaches a weed location* **then**
 9 **Drone State:** ANALYSIS The drone's sensors measure wind speed (V) and direction (θ).
 Compute the Reynolds number:

$$Re = \frac{\rho_{\text{air}} \cdot V_{\text{air}} \cdot (2r)}{\eta}$$

10 **if** $Re < 2000$ (*Laminar Flow*) **then**
 Spray Mode: LAMINAR Compute drift using Stokes' drag law (Eq. 1). Calculate displacement using kinematic equations (Eq. 10, Eq. 11). // The drone dynamically adjusts its position to counteract drift.
 12 **Drone State:** SPRAYING
 13 **else**
 14 **if** $2000 \leq Re < 4000$ (*Transitional Flow*) **then**
 Spray Mode: TRANSITIONAL Compute drag coefficient C_d using Eq. 3. Calculate drag force using the drag equation (Eq. 2). Compute displacement using kinematic equations (Eq. 10, Eq. 11). **Drone State:** SPRAYING
 16 **if** *Spraying task completed* **then**
 Drone State: EXPLORATION
 18 **else**
 19 **if** $Re \geq 4000$ (*Turbulent Flow*) **then**
 Spray Mode: TURBULENT // Displacement is computed iteratively with time step Δt .
 21 Compute Reynolds number Re and drag coefficient C_d . Calculate drag force F_d using Eq. 2. Update velocity:

$$V_x(\text{new}) = V_x(\text{old}) - \frac{F_d}{m} \Delta t$$

 Compute displacement incrementally:

$$x_{\text{drag}}+ = V_x \Delta t$$

 Sum displacements over droplet fall time. **Drone State:** SPRAYING
 22 **if** *Spraying task completed* **then**
 Drone State: EXPLORATION
 23 **else**
 24 **Spray Mode:** EXTREME TURBULENCE // Severe wind conditions detected; abort spraying.
 25 **Drone State:** FLYING // The drone returns to the base station.

27 **if** *All weed locations sprayed successfully* **then**
 28 **Drone State:** FLYING // The drone returns to its base station.
 29 **End of Algorithm.**

237 The drone enters an **Exploration** state as it starts navigation in the
238 field to the mapped weed locations. When it reaches a weed location, it
239 transitions into the **Analysis** state where it measures the current wind speed
240 and direction. Depending on the measured wind speed V , the Reynolds
241 number is calculated. As per the RE value, the drone adjusts its spray mode
242 as shown in Table 1, keeping the spray droplet radius at 0.0002m.

243 The drag force acting on the sprayed droplets is determined based on the
244 prevailing flow regime, which is classified as laminar, transitional, or turbulent
245 using the Reynolds number. Depending on the regime, the appropriate drag
246 coefficient is applied to compute the aerodynamic resistance experienced by
247 the droplets. Once the drag force is established, the displacement of the
248 droplets is calculated using kinematic equations that account for factors
249 such as wind speed, gravitational acceleration, and the initial velocity of the
250 droplets. To mitigate spray drift, the drone dynamically adjusts its position
251 in real-time. If the computed displacement indicates significant drift, the
252 drone compensates by repositioning itself in the opposite direction to ensure
253 accurate herbicide application. This adaptive correction enhances spray
254 precision, reduces chemical wastage, and minimizes unintended exposure to
255 non-target areas.

256 After spraying each location of the weeds, the drone checks if the task
257 is complete. If so, it transitions back to the **FLYING** state and moves to the
258 following weed location. Once all weed locations have been sprayed, the drone
259 switches to **Flying Mode** and returns to its base station.

260 4. Environmental setup

261 4.1. *Simulation Environment Development*

262 The proposed wind mitigation method was tested using an integrated
263 simulation platform developed with advanced tools including, the AirSim
264 simulator, PX4 SITL (PX4 Development Team, 2024), Unreal Engine
265 4, and ROS2 framework (Ma et al., 2020). All these tools collectively
266 simulated the UAV environment, featuring high-end functionalities in terms
267 of control, visualization, and real-world simulation. This integration ensured
268 a seamless workflow. Fig. 2 illustrates the interactions between the different
269 modules, including the transfer of control commands, sensor feedback, and
270 environmental dynamics.

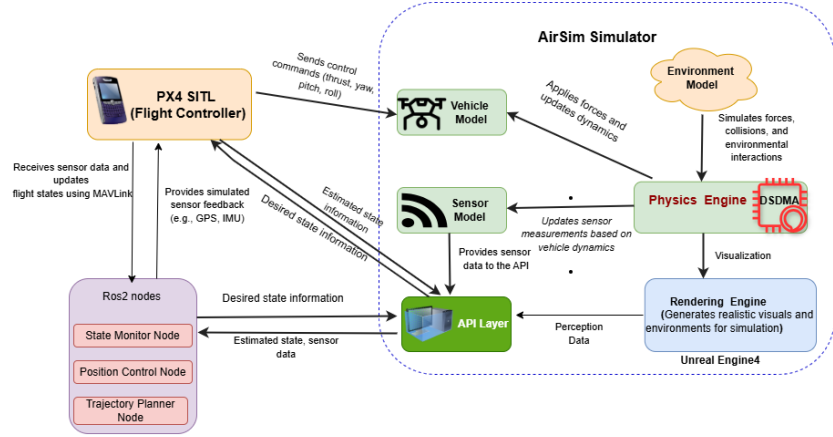


Fig. 2: Architecture of AirSim-UAV Simulation Framework Integrating PX4 SITL, Unreal Engine, and Various Models for Realistic Drone Simulation and Control

271 4.1.1. *AIRSim: Aerial Informatics and Robotics Simulation*

272 AIRSim (Microsoft Research, 2017b) is an open-source simulation
 273 environment. It has been created by Microsoft to support realistic simulation
 274 of autonomous vehicles, both UAVs and ground vehicles. It provides detailed
 275 and personalized 3D environments, such as cityscapes, forests, and open spaces,
 276 to simulate varied operational scenarios. The environment supports realistic
 277 flight dynamics, generation of sensor data, and environmental interaction,
 278 including wind effects, collision, and dynamic obstacles. AirSim uses an
 279 extensible, modular architecture based on the essential components of the
 280 environment, vehicle, physics engine, rendering engine, API layer, and sensor
 281 models. .

282 *Components.*

283 1. **Vehicle Model:** The vehicle model is a quadrotor drone with four rotors
 284 (Fig. 3a), intended to mimic the response of a real UAV. It includes
 285 a variety of simulated sensors such as an Inertial Measurement Unit
 286 (IMU) for orientation and acceleration, a barometer, GPU, cameras,
 287 and LiDAR. The UAV can either run in manual or autonomous mode.
 288 This research uses it in autonomous mode, which is controlled via the
 289 AirSim API and in conjunction with PX4 flight control software and
 290 MAVLink commands (Microsoft Research, 2017a).

291 2. **Virtual Agricultural Environment**

292 A virtual agrarian environment was created to support UAV
 293 experimentation and verification, as illustrated in Fig. 3b. The virtual
 294 environment simulates a natural agrarian field with crops and weeds
 295 scattered over a flat terrain. High-resolution textures were used on the
 296 terrain to simulate realistic soil and vegetation. This virtual environment
 297 allows UAVs to fly over the field while inter-working with other modules.



Fig. 3: A snapshot from AirSim shows an aerial vehicle flying in an agricultural environment.

298 *4.2. Physics Engine*

299 In the physical world, UAVs are acted upon by multiple physical forces
 300 like gravity, air density, air pressure, and magnetic fields. To correctly model
 301 them, these physical factors are inserted into the simulation's physics engine
 302 of AirSim(Cavalli, 2024) The proposed DSDMA algorithm was also integrated
 303 into the simulation's physics engine for dynamic spray drift mitigation. All
 304 parameters used to replicate real-world environmental conditions in the
 305 simulation are as follows:

306 **1. Gravity:** In the AirSim simulation environment, gravity (g) is typically
 307 treated as constant with a value of $g = 9.8 \text{ m/s}^2$, assuming the simulation
 308 occurs close to the Earth's surface where variations in g due to altitude
 309 (h) are negligible(Cavalli, 2024). However, if altitude-based variations
 310 in g need to be accounted for, the following equation is incorporated
 311 into the physics engine:

$$g = g_0 \cdot \frac{R_e^2}{(R_e + h)^2} \approx g_0 \cdot \left(1 - 2 \frac{h}{R_e}\right)$$

312 Where: g : gravitational acceleration at height h , g_0 : gravitational
 313 acceleration at Earth's surface, R_e : Earth's radius, h : height above
 314 Earth's surface.

315 2. **Air pressure and density:** In the AirSim simulation environment, air
316 pressure and air density are not explicitly modeled by default. However,
317 these parameters are crucial in determining the lift, drag, and propulsion
318 forces acting on a UAV or drone. The relationship between the altitude
319 and the pressure of the Earth’s atmosphere is complicated due to many
320 distinct layers, each with its individual properties(Cavalli, 2024). The
321 air density is given by:

$$\rho = \frac{P}{R \cdot T}$$

322 Where R is the specific gas constant.

323 4.3. *Sensor Models*

324 AirSim has multiple sensor models for accelerometer, gyroscope, barometer,
325 magnetometer, and GPS. We employed a gyroscope, accelerometer, and GPS
326 in this research. The gyroscope and accelerometer are basic sensors and the
327 core part of the Inertial Measurement Unit (IMU). The gyroscope detects
328 the angular speed (rate of spin) of the drone about its primary axes—roll,
329 pitch, and yaw. Accelerometer is used to measure the linear acceleration
330 of the drone in the three axes (X,Y,Z). GPS sensor mimics the position of
331 an autonomous aerial vehicle. Precise GPS position information is needed
332 for navigation, mission planning, and ensuring precise movement within the
333 simulated environment.

334 4.4. *PixHawk4 Software-in-the-Loop (PX4-SITL):*

335 PX4-SITL(Microsoft, 2017) is a flight control software that manages flight
336 motion in the simulation environment. PX4 communicates with the drone
337 using a protocol known as MAVLink. Therefore, PX4 emulates the UAV
338 sensors and dynamics and is a critical tool for testing flight control algorithms
339 and software.

340 4.5. *Robotic Operating System (ROS2)*

341 ROS2(Macenski et al., 2022) forms the core middleware between PX4 SITL
342 and the simulator AirSim, enabling seamless communication and computations
343 using its distributed node-based structure. The intended study employs several
344 major nodes: the State Monitor Node, which monitors the UAV’s velocity,
345 position, and drift during simulation by processing UE4 telemetry feedback;
346 the Position Control Node, which keeps the UAV’s course by compensating
347 for environmental disruptions such as wind; the Error Node, which senses

348 and deals with deviations, malfunctions, and sensor errors, alerting the
349 user interface and initiating corrective measures when appropriate; and the
350 Trajectory Planner Node, which works in tandem with the Position Control
351 Node to compute optimal trajectories and smooth out navigation to waypoints.

352 5. Results and discussion

353 5.1. Drone Path and Initial Conditions

354 Initially, the drone was instructed to follow a few predefined waypoints,
355 assuming the weeds' locations. These coordinates represent the drone's
356 path at a constant altitude of -20 meters. To simulate real-world scenarios,
357 external wind disturbances were introduced with varying speeds, directions,
358 and flow conditions (laminar, transitional, and turbulent). These disturbances
359 significantly affected the drone's spraying accuracy, as reflected in the drift
360 results summarized in Table 2. The table captures six cases, each characterized
361 by a distinct wind speed and wind direction (ranging from 30° to 70°). The
362 wind speed range from 1.5 m/s to 7.0 m/s was chosen to reflect realistic
363 field conditions for UAV-based agricultural spraying. Studies in precision
364 agriculture and aerial spraying regulations suggest that UAV spraying should
365 ideally occur within this wind speed range to maintain droplet control while
366 ensuring operational efficiency (Volitant Technologies, 2025).

367 The original waypoints represent the UAV's planned spraying locations in
368 wind-free conditions. However, droplet displacement necessitates adjustments
369 to these waypoints in the presence of wind. The adjusted waypoints shift the
370 UAV's position upwind, compensating for drift to ensure the spray reaches
371 its intended target. The magnitude of these adjustments increases with
372 wind speed and direction, as evident in Case 1 (1.5 m/s, 30° wind direction),
373 where minor corrections are required, compared to Case 6 (7.0 m/s, 70° wind
374 direction), where substantial repositioning is necessary.

375 The findings validate that DSDMA successfully reduces drift by
376 dynamically adjusting UAV locations to offset wind influences, improving
377 spraying accuracy. The correction method guarantees herbicides are effectively
378 delivered on target crops, minimizing off-target contamination and enhancing
379 overall agricultural sustainability. The results also demonstrate that
380 integrating real-time wind compensation into UAV-based spraying systems
381 significantly enhances operational accuracy, making DSDMA a robust solution
382 for precision agriculture. (Volitant Technologies, 2025).

Table 2: Wind and flow characteristics with waypoint adjustments

Case	Wind Speed (m/s)	Wind Direction (°)	Droplet Radius (m)	Reynolds Number	Flow Type	Original Waypoint	Adjusted Waypoint
1	1.5	30.0	0.0002	20.30	Laminar	[30 0 -20] [30 30 -20] [0 30 -20] [0 0 -20]	[19.42 -6.11 -20] [19.42 23.89 -20] [-10.58 23.89 -20] [-10.58 -6.11 -20]
2	2.0	40.0	0.0002	27.07	Laminar	[30 0 -20] [30 30 -20] [0 30 -20] [0 0 -20]	[17.52 -10.47 -20] [17.52 19.53 -20] [-12.48 19.53 -20] [-12.48 -10.47 -20]
3	2.5	50.0	0.0002	33.84	Laminar	[30 0 -20] [30 30 -20] [0 30 -20] [0 0 -20]	[16.91 -15.60 -20] [16.91 14.40 -20] [-13.09 14.40 -20] [-13.09 -15.60 -20]
4	3.0	60.0	0.0002	40.61	Laminar	[30 0 -20] [30 30 -20] [0 30 -20] [0 0 -20]	[17.78 -21.16 -20] [17.78 8.84 -20] [-12.22 8.84 -20] [-12.22 -21.16 -20]
5	3.2	70.0	0.0002	43.31	Laminar	[30 0 -20] [30 30 -20] [0 30 -20] [0 0 -20]	[21.09 -24.49 -20] [21.09 5.51 -20] [-8.91 5.51 -20] [-8.91 -24.49 -20]
6	7.0	70.0	0.0002	94.75	Laminar	[30 0 -20] [30 30 -20] [0 30 -20] [0 0 -20]	[10.5 -53.58 -20] [10.5 -23.58 -20] [-19.5 -23.58 -20] [-19.5 -53.58 -20]

383 The proposed DSDMA algorithm is theoretically capable of adapting to
 384 various flow regimes, including laminar, transitional, and turbulent conditions;
 385 however, the current study focuses on laminar flow, as UAV operations
 386 remain effective and droplet motion predictable within wind speeds up to 10
 387 m/s. UAV operational limits and real-world agricultural spraying conditions
 388 constrain its practical implementation. However, future work could explore
 389 wind tunnel experiments or large-scale simulations to evaluate the algorithm's
 390 performance in higher wind conditions, independent of UAV constraints. The
 391 visual representation of UAV's drift under varying wind conditions is shown in
 392 Fig.4. Each subfigure corresponds to one of the cases, illustrating the impact
 393 of wind speed and direction on the drone's trajectory.

394 *5.2. Quantitative Validation of the DSDMA Algorithm: Mean Absolute Error
 395 (MAE) Analysis*

396 To measure the algorithm's effectiveness quantitatively, we computed the
 397 Mean Absolute Error (MAE) between the original target positions and the
 398 actual spray impact locations before and after correction. The MAE is defined
 399 as

$$\text{MAE} = \frac{1}{n} \sum_{i=1}^n |P_{\text{original},i} - P_{\text{actual},i}| \quad (28)$$

400 where:

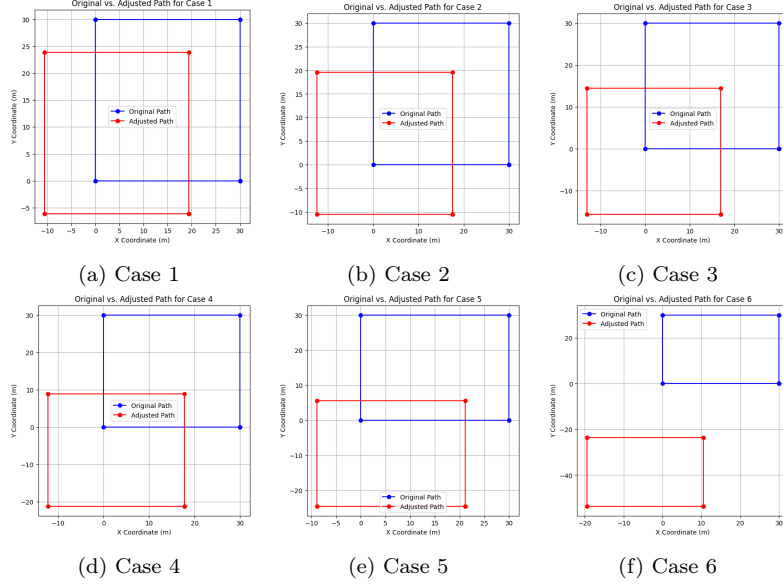


Fig. 4: Different cases of wind speed and wind direction applied

- 401 • n : Total number of waypoints or samples.
- 402 • $P_{\text{original},i}$: The original (target) position of the spray point.
- 403 • $P_{\text{actual},i}$: The actual or adjusted spray position after applying DSDMA.
- 404 The MAE values for each case, representing the deviation of the drone from
405 its original position due to wind effects, are given in Table 3

Table 3: Mean Absolute Error (MAE) of Droplet Drift Compensation Using DSDMA

Case	Wind Speed (m/s)	MAE (m)
Case 1	1.5	5.56
Case 2	2.0	7.65
Case 3	2.5	9.56
Case 4	3.0	11.13
Case 5	3.2	11.13
Case 6	7.0	24.36

- 406 The MAE quantitatively measures the average deviation between the
407 target spray locations (original waypoints) and the corrected UAV positions

408 (adjusted waypoints) from which spraying is performed. The algorithm's
409 performance to counteract wind-induced drift is measured by calculating
410 the MAE for all test cases. The lower the MAE value, the smaller the
411 correction distance, implying the spray hits its desired target with much
412 less deviation. On the other hand, a greater MAE indicates stronger wind
413 conditions necessitating greater positional corrections. This linear relationship
414 shows how effectively the DSDMA accounts for different wind conditions,
415 enhances overall spraying efficiency, lowers herbicide loss, and lessens off-target
416 environmental effects. The validation based on MAE thus proves DSDMA
417 to be a scientifically sound and practically feasible solution for precision
418 agriculture.

419

420 6. Conclusion

421 This study introduces an aerodynamics-inspired framework to mitigate
422 the impact of wind on UAV spraying in precision agriculture. To achieve this,
423 a Dynamic Spray Drift Mitigation Algorithm (DSDMA) is proposed, which
424 dynamically adjusts the UAV's position in real time by incorporating wind
425 speed, direction, and flow regimes into its calculations. Unlike traditional
426 static spray methods, the algorithm guarantees the consistent delivery of
427 droplets to their targets, enhancing deposition accuracy and improving
428 environmental health. To further improve stability and trajectory control in
429 spraying operations, a Proportional-Integral-Derivative (PID) controller was
430 incorporated with DSDMA. This improved the drone's capability to sustain
431 corrected positions in varying wind conditions with minimal deviation and
432 strong path following.

433 The proposed system was thoroughly tested in a high-fidelity simulation
434 environment, integrating advanced tools such as the AirSim simulator, ROS2,
435 PX4, and Unreal Engine. The simulation setup featured an agricultural
436 scenario with a UAV operating in realistic conditions. Results provided an
437 optimal position of the drone to spray so that there is minimum spray drift.
438 Mean Absolute Error (MAE), confirming the algorithm's ability to counteract
439 drift under laminar flow conditions. While the algorithm applies to all flow
440 regimes (laminar, turbulent, transitional), real-world UAV limitations prevent
441 operation beyond laminar conditions, which apply to real-world agricultural
442 spraying. In general, DSDMA improves the accuracy of agrochemical delivery
443 and helps in sustainable agriculture by reducing off-target drift and chemical

444 excess. This research forms the basis for the future generation of smart
445 spraying systems. Future research may investigate wind tunnel experiments
446 or large-scale simulations to analyze the algorithm's performance under higher
447 wind conditions, irrespective of UAV limitations. It could involve extensive
448 field testing at large scales, algorithm tuning for challenging landscapes, and
449 further integrating AI-supported adaptive decision-making to enhance the
450 influence of DSDMA in practical agricultural contexts.

451 **Statements and Declarations**

452 *Competing Interests*

453 The authors declare that they have no known competing financial interests
454 or personal relationships that could have appeared to influence the work
455 reported in this paper.

456 *Author Contributions*

457 **Rajni Goyal:** Writing – original draft, Software, Methodology,
458 Data curation. **Srinjoy Chakraborty:** Methodology, Experimentation,
459 Conceptualization. **Amar Nath:** Writing – review & editing, Supervision,
460 Project administration. **Utkarsh Niranjan:** Visualization, Supervision.

461 **References**

- 462 Alexandratos, N., & Bruinsma, J. (2012). World agriculture towards
463 2030/2050: the 2012 revision.
- 464 Anderson, J. (2011). EBOOK: Fundamentals of Aerodynamics (SI units).
465 McGraw hill.
- 466 An, D., Hollenbeck, D., Cao, K., & Chen, Y. (2023). Soil methane emission
467 suppression control using unmanned aircraft vehicle swarm application of
468 biochar mulch-A simulation study. Journal of Information and Intelligence,
469 1(1), 68-85.
- 470 Bagchi, P., & Balachandar, S. (2003). Effect of turbulence on the drag and
471 lift of a particle. Physics of fluids, 15(11), 3496-3513.

- 472 Bennetts, V. H., Kucner, T. P., Schaffernicht, E., Neumann, P. P., Fan, H.,
473 & Lilienthal, A. J. (2017). Probabilistic air flow modelling using turbulent
474 and laminar characteristics for ground and aerial robots. *IEEE robotics*
475 and automation letters
- 476 Birouk, M., & Abou Al-Sood, M. M. (2007). Numerical study of sphere
477 drag coefficient in turbulent flow at low Reynolds number. *Numerical Heat*
478 *Transfer, Part A: Applications*, 51(1), 39-57.
- 479 Bottema, O., & Roth, B. (1990). *Theoretical kinematics* (Vol. 24). Courier
480 Corporation.
- 481 Boychev, I. Z. (2018, September). Research algorithms to optimize the
482 drone route used for security. In *2018 IEEE XXVII International Scientific*
483 *Conference Electronics-ET* (pp. 1-4). IEEE.
- 484 Cavalli, A. (2024). Development of a simulation environment for precision
485 agriculture applications with Unmanned Aircraft Systems (Doctoral
486 dissertation, Politecnico di Torino).
- 487 Chen, Y., Hou, C., Tang, Y., Zhuang, J., Lin, J., & Luo, S. (2019). An effective
488 spray drift-reducing method for a plant-protection unmanned aerial vehicle.
489 *International Journal of Agricultural and Biological Engineering*, 12(5),
490 14-20.
- 491 Chen, S., Lan, Y., Zhou, Z., Ouyang, F., Wang, G., Huang, X., ... & Cheng,
492 S. (2020). Effect of droplet size parameters on droplet deposition and drift
493 of aerial spraying by using plant protection UAV. *Agronomy*, 10(2), 195.
- 494 Chen, S., Lan, Y., Zhou, Z., Deng, X., & Wang, J. (2021). Research advances
495 of the drift reducing technologies in application of agricultural aviation
496 spraying. *International Journal of Agricultural and Biological Engineering*,
497 14(5), 1-10.
- 498 Chowdhury, S., Shahvari, O., Marufuzzaman, M., Li, X., & Bian, L. (2021).
499 Drone routing and optimization for post-disaster inspection. *Computers &*
500 *Industrial Engineering*, 159, 107495.
- 501 Clift, R., Grace, J. R., & Weber, M. E. (2005). *Bubbles, drops, and particles*.

- 502 Dorling, K., Heinrichs, J., Messier, G. G., & Magierowski, S. (2016). Vehicle
503 routing problems for drone delivery. *IEEE Transactions on Systems, Man,
504 and Cybernetics: Systems*, 47(1), 70-85.
- 505 Faiçal, B. S., Pessin, G., Filho, G. P., Carvalho, A. C., Gomes, P. H., &
506 Ueyama, J. (2016). Fine-tuning of UAV control rules for spraying pesticides
507 on crop fields: An approach for dynamic environments. *International
508 Journal on Artificial Intelligence Tools*, 25(01), 1660003.
- 509 Faiçal, B. S., Freitas, H., Gomes, P. H., Mano, L. Y., Pessin, G., de Carvalho,
510 A. C., ... & Ueyama, J. (2017). An adaptive approach for UAV-based
511 pesticide spraying in dynamic environments. *Computers and Electronics in
512 Agriculture*, 138, 210-223.
- 513 Felsot, A. S., Unsworth, J. B., Linders, J. B., Roberts, G., Rautman, D.,
514 Harris, C., & Carazo, E. (2010). Agrochemical spray drift; assessment and
515 mitigation—A review. *Journal of Environmental Science and Health Part
516 B*, 46(1), 1-23.
- 517 Ferguson, J. C., O'Donnell, C. C., Chauhan, B. S., Adkins, S. W., Kruger, G.
518 R., Wang, R., ... & Hewitt, A. J. (2015). Determining the uniformity and
519 consistency of droplet size across spray drift reducing nozzles in a wind
520 tunnel. *Crop Protection*, 76, 1-6.
- 521 Genç, M. S. (Ed.). (2012). Low Reynolds Number: Aerodynamics and
522 Transition. BoD—Books on Demand.
- 523 Greenblatt, D., & Williams, D. R. (2022). Flow control for unmanned air
524 vehicles. *Annual Review of Fluid Mechanics*, 54(1), 383-412.
- 525 Johnson, M. A., & Moradi, M. H. (2005). PID control (pp. 47-107). London,
526 UK: Springer-Verlag London Limited.
- 527 Kethineni, K. K., Mohanty, S. P., Kougianos, E., Bhowmick, S., & Rachakonda,
528 L. (2024). SprayCraft: Graph-Based Route Optimization for Variable Rate
529 Precision Spraying. *arXiv preprint arXiv:2412.12176*.
- 530 Li, Y., Ang, K. H., & Chong, G. C. (2006). PID control system analysis and
531 design. *IEEE Control Systems Magazine*, 26(1), 32-41.

- 532 Liu, Q., Shan, C., Zhang, H., Song, C., & Lan, Y. (2023). Evaluation of liquid
533 atomization and spray drift reduction of hydraulic nozzles with four spray
534 adjuvant solutions. *Agriculture*, 13(2), 236.
- 535 Macenski, S., Foote, T., Gerkey, B., Lalancette, C., & Woodall, W. (2022).
536 Robot operating system 2: Design, architecture, and uses in the wild.
537 *Science robotics*, 7(66), eabm6074.
- 538 Ma, C., Zhou, Y., & Li, Z. (2020, April). A new simulation environment
539 based on AirSim, ROS, and PX4 for quadcopter aircrafts. In 2020 6th
540 international conference on control, automation and robotics (ICCAR) (pp.
541 486-490). IEEE.
- 542 Marubayashi, R. Y., Oliveira, R. B. D., Ferreira, M. D. C., Roggia, S.,
543 Moraes, E. D. D., & Saab, O. J. (2021). Insecticide spray drift reduction
544 with different adjuvants and spray nozzles. *Revista Brasileira de Engenharia
545 Agrícola e Ambiental*, 25, 282-287.
- 546 Microsoft, “PX4 SITL integration,” [Online]. Available:
547 https://microsoft.github.io/AirSim/px4_sitl/.
- 548 Microsoft Research, “Vehicle selection API,” 2017. [Online]. Available:
549 <https://microsoft.github.io/AirSim/apis/>.
- 550 Microsoft Research, “AirSim: A simulation platform for AI research and
551 experimentation,” [Online]. Available: <https://microsoft.github.io/AirSim/>.
552 [Accessed: Dec. 31, 2024].
- 553 PX4 Development Team, “Gazebo Simulation PX4
554 v1.9.0 Developer Guide,” [Online]. Available:
555 https://dev.px4.io/v1.9.0_noredirect/en/simulation/gazebo.html.
556 [Accessed: Dec. 31, 2024].
- 557 Scagnellato, L. (2022). Multi-rotor UAS for precision crop-spraying:
558 developing an adaptive guidance algorithm to minimize spray drift in
559 a wind environment (Doctoral dissertation, Politecnico di Torino).
- 560 Sánchez-Fernández, L., Barrera, M., Martínez-Guanter, J., & Pérez-Ruiz, M.
561 (2023). Drift reduction in orchards through the use of an autonomous UAV
562 system. *Computers and Electronics in Agriculture*, 211, 107981.

- 563 Shyy, W., Lian, Y., Tang, J., Viieru, D., & Liu, H. (2008). Aerodynamics of
564 low Reynolds number flyers.
- 565 Srivastava, K., Pandey, P. C., & Sharma, J. K. (2020). An approach for route
566 optimization in applications of precision agriculture using UAVs. *Drones*,
567 4(3), 58.
- 568 Volitant Technologies. (2025). Agras T40 quick specs. Retrieved April 11,
569 2025, from <https://volitantdrones.com/agras-t40-quick-specs/>
- 570 Wang, C., Zeng, A., He, X., Song, J., Andreas, H., & Gao, W. (2020). Spray
571 drift characteristics test of unmanned aerial vehicle spray unit under wind
572 tunnel conditions. *International Journal of Agricultural and Biological
573 Engineering*, 13(3), 13-21.
- 574 Wang, G., Han, Y., Li, X., Andaloro, J., Chen, P., Hoffmann, W. C., ... &
575 Lan, Y. (2020). Field evaluation of spray drift and environmental impact
576 using an agricultural unmanned aerial vehicle (UAV) sprayer. *Science of
577 the Total Environment*, 737, 139793.

Change Log

* elsarticle.dtx

1. `global\bibsep=0pt` commented out for all models since it produced error for all `\jtype` options.
 2. The error "`!LaTeX Error: Command \c@author already defined.`" has been resolved by updating `elsarticle.dtx`.
-



Click here to access/download
LaTeX Source Files
elsarticle-harv.bst



Click here to access/download
LaTeX Source Files
elsarticle-num-names bst



Click here to access/download
LaTeX Source Files
`elsarticle-num.bst`



Click here to access/download
LaTeX Source Files
`elsarticle-template-harv.tex`





Click here to access/download
LaTeX Source Files
`elsarticle-template-num-names.tex`



Click here to access/download
LaTeX Source Files
elsarticle.dtx



Click here to access/download
LaTeX Source Files
`elsarticle.ins`



Click here to access/download
LaTeX Source Files
manifest.txt



Click here to access/download
LaTeX Source Files
README



Declaration of interests

The authors declare that they have no known competing financial interests or personal relationships that could have appeared to influence the work reported in this paper.

The authors declare the following financial interests/personal relationships which may be considered as potential competing interests: